Thin Germanium Waveguide-Array-Like Absorber Based on Localized Resonance

Yijin Zhang, Xiyuan Cao, Xiaoyu Liu, Li Liu, Longsheng Wu, Jian Sun, Zhongying Xue, Yi Jin, and Aimin Wu

***Abstract*—Mode overlapping promotes the capability in manipulating optical absorption. Based on such a mechanism, an all-dielectric metasurface has the capability of perfectly absorbing incident optical energy without the assistance of a mirror. Here, an array of thin germanium waveguide-like units is designed as a special absorber possessing some advantages by overlapping two localized resonant modes. Such a thin absorber can realize strong absorption even though the germanium material is of low loss at the *O* band. It is found that the absorption capability is about three times stronger than that of an unpatterned germanium film with the same thickness, and wideband strong absorption is obtained at the same time. The structure is continuous so that it can conduct carriers in photodetection. The suggested method would be heuristic in the photodetection area.**

***Index Terms*—Perfect absorption, waveguide-like, dielectric metasurface, localized resonance.**

I. Introduction

SINCE the conception of metamaterial absorbers was raised [1], [2], the capability in manipulating optical absorption has been put forward in a large step. A typical metamaterial absorber (MA) consists of one patterned metal layer, one dielectric spacer and a metal substrate [3]–[5]. Under the assistance of the metal substrate as a reflecting mirror, it is easy to realize perfect absorption based on the resonance from each unit. With a thin thickness, a MA can be scaled to operate in different frequency bands from the microwave to the ultraviolet [6].The central working frequency can be adjusted by introducing some tunable materials or mechanisms [7], and the working bandwidth can also be designed to be broadband based on various mechanisms, especially by introducing several different resonant modes into one unit cell [8]–[12]. MAs have been applied in various areas, such as electromagnetic and infrared cloaking [13], [14], photoelectric detection and imaging [15]–[17], solar energy utilization [18]–[20] and sensitive sensing [21]–[23]. Now, it is hoped to extend traditional MAs to realize new-type absorbers for particular applications based on mode overlapping. Commonly, a thin dielectric layer can only trap a limited part of incident optical energy. Dielectric photonic crystals may achieve perfect absorption when they support two leaky guided modes at the same time [24]–[26]. However, the operating bandwidth is narrow and the absorption performance is sensitive to the existence of a supporting dielectric substrate. These problems can be overcome by high-index dielectric nanoantennas. As an absorbing metasurface, an array of dielectric nanoantennas sustaining two localized resonant modes simultaneously may also achieve perfect absorption without a reflecting mirror [27]–[29]. All-dielectric absorbers are especially significant in photodetection without the complex design and thermal energy of metals, which can help realize a high-efficiency detector with high responsivity and fast response.

High-performance near-infrared photodetectors are one key component in the optical interconnect technology which is one effective way to solve the growing demand for data transfer. At present, commercial photodetectors in the optical communication are mainly based on III-V compound semiconductors [30], [31], which are not suitable for large-scale integration. Recently, germanium (Ge) has gained extensive attention as a complementary-metal-oxide-semiconductor (CMOS) compatible material [32], which is promising for optical detection. For now, surface-illuminated Ge photodetectors have been already used in datacom and telecom, which face the bandwidth-efficiency trade-off. Designing a thin Ge absorber integrated in a photodetector is an effective way to improve the device performance.

Although an array of discrete Ge nanoantennas can perform perfect absorption, they can't conduct produced carriers laterally in photodetection. In this work, we propose a design paradigm of a thin all-dielectric absorber based on the Ge-on-Insulator (GOI) platform which can avoid such a problem. An array of

Manuscript received 1 July 2022; accepted 7 July 2022. Date of publication 18 July 2022; date of current version 10 August 2022. This work was supported in part by the National Natural Science Foundation of China under Grant 61875174, in part by the Youth Innovation Promotion Association of the Chinese Academy of Sciences under Grant 2021232, and in part by the Shanghai Sailing Program under Grant 19YF1456600. *(Corresponding authors: Yi Jin; Aimin Wu.)*

Yijin Zhang, Xiaoyu Liu, Li Liu, Longsheng Wu, Zhongying Xue, and Aimin Wu are with the State Key Laboratory of Functional Materials for Informatics, Shanghai Institute of Microsystem and Information Technology, Chinese Academy of Sciences, Shanghai 200050, China, and also with the Center of Materials Science and Optoelectronics Engineering, University of Chinese Academy of Sciences, Beijing 100049, China (e-mail: yjzhang@mail.sim.ac.cn; xiaoyuliu@mail.sim.ac.cn; liul3104@mail.sim.ac.cn; wls502852331@mail.sim.ac.cn; simsnow@mail.sim.ac.cn; wuaimin@mail.sim.ac.cn).

Xiyuan Cao is with the State Key Laboratory of Dynamic Measurement Technology, North University of China, Taiyuan 030000, China (e-mail: caoxiyuan@nuc.edu.cn).

Jian Sun is with the Engineering Research Center of Ultra-Precision Optical Manufacturing (Shanghai), Department of Optical Science and Engineering, School of Information Science and Technology, Fudan University, Shanghai 200433, China (e-mail: jsun@fudan.edu.cn).

Yi Jin is with the Centre for Optical and Electromagnetic Research and International Research Center for Advanced Photonics, College of Optical Science and Engineering, Zhejiang University, Hangzhou 310058, China (e-mail: jinyi_2008@zju.edu.cn).

This article has supplementary downloadable material available at https://doi.org/10.1109/JPHOT.2022.3190138, provided by the authors.

Digital Object Identifier 10.1109/JPHOT.2022.3190138

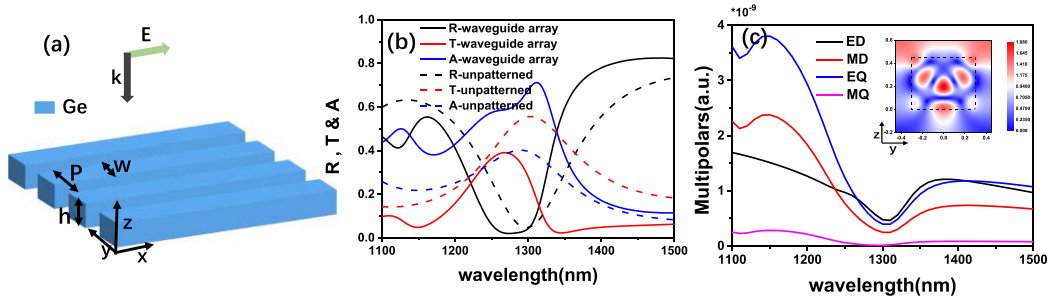

Fig. 1. Ge waveguide-array absorber in free space. (a) Structure configuration. (b) Transmission, reflection and absorption for normal TE incidence. $P = 900$ nm, $w = 600$ nm and $h = 450$ nm. When the Ge waveguide array is replaced by an unpatterned Ge film of the same thickness, the corresponding scattering response is also given. (c) Multipolar decomposition of the scattering cross-sections for the waveguide array. The inset shows the normalized electric amplitude distribution on the cross section of one strip waveguide at wavelength 1310 nm.

deformed continuous Ge waveguides is used to realize perfect absorption by overlapping two localized resonant modes, which does not require a reflecting mirror. The thin absorber can work operate at long wavelengths where Ge is of low material loss. This work paves a new way for high-responsivity and high-speed photodetectors with a thin intrinsic layer.

II. Results and Discussion

First, an array of Ge strip waveguides in free space is investigated as an absorber, which is illustrated in Fig. 1(a). The period of the waveguide array is P, and the width and thickness of each strip waveguide are w and h, respectively. For demonstration, the absorption (A), reflection (R) and transmission (T) for an optimized case is shown in Fig. 1(b) when $P = 900$ nm, $w = 600$ nm and $h = 450$ nm. The incident light impinges normally downward with the electric field polarized along the x axis (TE incidence). Numerical simulation is performed based on the finite-difference time-domain method (Lumerical software), and the material parameter of Ge is fitted by Palik's model [33]. There is an obvious absorption peak at wavelength 1310 nm and the absorption is up to $A = 73\%$ although the Ge material loss is low at this wavelength. As a comparison, Fig. 1(b) also shows the absorption spectra for an unpatterned Ge film of the same thickness. The absorption of the homogeneous Ge film is weak, and the absorption peak induced by the Fabry-Pérot resonance between the up and bottom film interfaces is only about 40%, which deviates a bit from wavelength 1310 nm.

In order to qualitatively understand the strong absorption of the Ge waveguide array, the multipolar decomposition [34] of scattering cross-sections is performed by using the finite element method (COMSOL Multiphysics). One can observe the respective contributions from the electric dipole (ED), the magnetic dipole (MD), the electric quadrupole (EQ) and the magnetic quadrupole (MQ) in Fig. 1(c). The contribution of the MQ is negligible, and the contributions of ED, MD and EQ to the scattering response of the waveguide array have a consistent trend around wavelength 1310 nm and reach a minimum at the absorption peak. The ED just approaches to the MD in the strength, but can't match it. This makes the waveguide array unable to realize perfect absorption, although strong absorption can be reached [35]. This is consistent with the common conclusion that perfect absorption may be achieved when the ED is the same as the MD in the strength [36]. The normalized electric amplitude distribution on the cross section of one strip waveguide at wavelength 1310 nm is shown in Fig. 1(c). One can see that the electric field is mainly localized inside the dielectric structure to help realizing strong absorption.

In order to realize perfect absorption, a Ge waveguide-array-like absorber derived from the above investigated one is designed, which is illustrated in Fig. 2(a). Narrow Ge arms are added vertical to each strip axis in a fixed separation of P_x, of which the width is w_x and the length is L. For distinction, the width of each strip waveguide is labeled as w_y and the period of the strip array is labeled as P_y newly. When it is assumed that $P_y = P_x = 800$ nm, $h = 450$ nm, $w_y = 310$ nm, $w_x = 210$ nm, and $L = 573$ nm, the absorption of the derived absorber is shown in Fig. 2(b) for normal TE incidence. Due to the introduction of the side arms, the absorption is obviously enhanced in a broad bandwidth, that is, the absorption between 1100 nm and 1340 nm is over 60%, superior to that of the above waveguide array. This broadband strong absorption is fascinating in photodetection. Especially, perfect absorption can be achieved now, one can note that strong absorption of about 98.4% at wavelength 1310 nm is obtained now. Compared with the traditional methods in obtaining strong absorption, such as adding an anti-reflection coating, the current absorber can achieve perfect absorption just based on a patterned thin intrinsic layer.

To understand the perfect absorption, the multipolar decomposition result for the waveguide-array-like absorber is shown in Fig. 2(c). Different from the waveguide-array one, the contributions of the ED, MD and EQ to the scattering response of the current one no longer follow the same trend in the near infrared. The introduction of side arms efficiently adjusts the respective strengths of the three multipoles. The ED and the MD is comparative near wavelength 1310 nm while the EQ is relatively weak. Thus, perfect absorption can be realized by deforming the waveguide array. The inset of Fig. 2(c) shows the normalized electric amplitude distribution on the transverse cross section of one deformed waveguide at wavelength 1310 nm, indicating more confined field localization.

To have a further qualitative understanding of the perfect absorption of the waveguide-array-like absorber, the influence of various geometrical parameters, including P_y, h, and w_y,

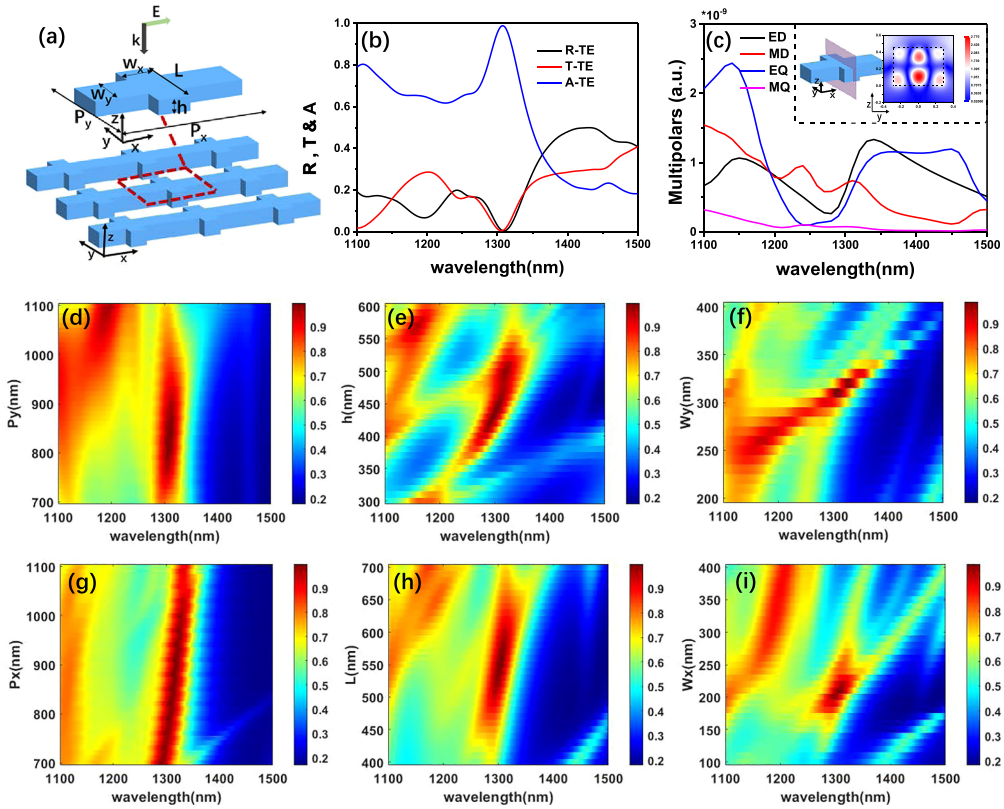

Fig. 2. Ge waveguide-array-like absorber in free space. (a) Structure configuration. The inset is the magnified view of one unit cell. (b) Transmission, reflection and absorption for normal TE incidence. $P_x = P_y = 800$ nm, $h = 450$ nm, $w_y = 310$ nm, $w_x = 210$ nm, and $L = 573$ nm. (c) Multipolar decomposition of the scattering cross-sections for the waveguide-array-like absorber. The inset shows the normalized electric amplitude distribution on the cross section of one strip waveguide at wavelength 1310 nm. (d)–(i) Influence of varying P_y, h, w_y, P_x, L and w_x on the absorption.

on the absorption are investigated as shown in Fig. 2(d)–(f). As can be seen in Fig. 2(d), the absorption peak is hardly affected by P_y. This confirms that the perfect absorption is induced by localized resonance instead of periodic coupling. The geometrical parameters of h and w_y directly determine the property of localized resonance, and the absorption behavior is altered following their variation. In Fig. 2(e) and (f), one can observe that the perfect absorption peak splits into two strong absorption peaks as shifting h and w_y from their optimized values of 450 nm and 310 nm, respectively. This indicates that two localized resonant modes supported by each deformed Ge strip waveguide cooperatively lead to the perfect absorption peak. The Ge side arms help one make the corresponding ED and MD matched when the two localized resonant modes overlap at wavelength 1310 nm. Then, the influence of the left geometrical parameters of P_x, L, and w_x on the absorption is also investigated as shown in Fig. 2(g)–(i). Because the excited field is mainly localized inside the dielectric structure, unlike P_y, the variation of P_x influences the position of the absorption peak as shown in Fig. 2(g), but in a weak way. The side arms can induce the appearance of perfect absorption, thus both L and w_x can also influence the perfect absorption. Like w_y, the shift of w_x from the optimized value splits the perfect absorption peak into two strong absorption ones, which further illustrates that the perfect absorption comes from the cooperation between two localized resonant modes.

In practice, the waveguide-array-like absorber is required to be supported by a substrate for fabrication convenience. It is assumed that the absorber is put on a standard silicon (Si) substrate with a 1.04 μm silica (SiO_2) spacer as shown in Fig. 3(a). The existence of such a substrate may disturb the absorption behavior. To obtain perfect absorption, the various geometrical parameters are necessary to be adjusted in a small degree. When $P_x = P_y = 800$ nm, $w_x = 200$ nm, $L = 590$ nm, $w_y = 310$ nm, $h = 450$ nm, Fig. 3(b) shows the scattering behavior of the substrated absorber for normal TE incidence. Perfect absorption of about 99.8% is obtained near 1310 nm, which is about 3 times stronger than that of an unpatterned Ge film with the same thickness, and broadband strong absorption is still maintained.

In the following, the absorption sensitivity to oblique incidence is investigated and the result is shown in Fig. 3(c) and (d). As illustrated by the inset of Fig. 3(c), the incident angle of θ is varied along the y-z plane and the incident electric filed is fixed along the x direction in Fig. 3(c). When θ is small, the absorption is insensitive to small θ since the strong absorption is from the localized resonance, but it decreases rapidly when θ tends to the first-order diffraction inside the SiO_2 spacer induced by the transverse period of P_y. And as illustrated by the inset of Fig. 3(d), the incident angle of θ is varied along the x-z plane and the incident magnetic field is fixed along the y direction in Fig. 3(d). The absorption is also insensitive to such oblique

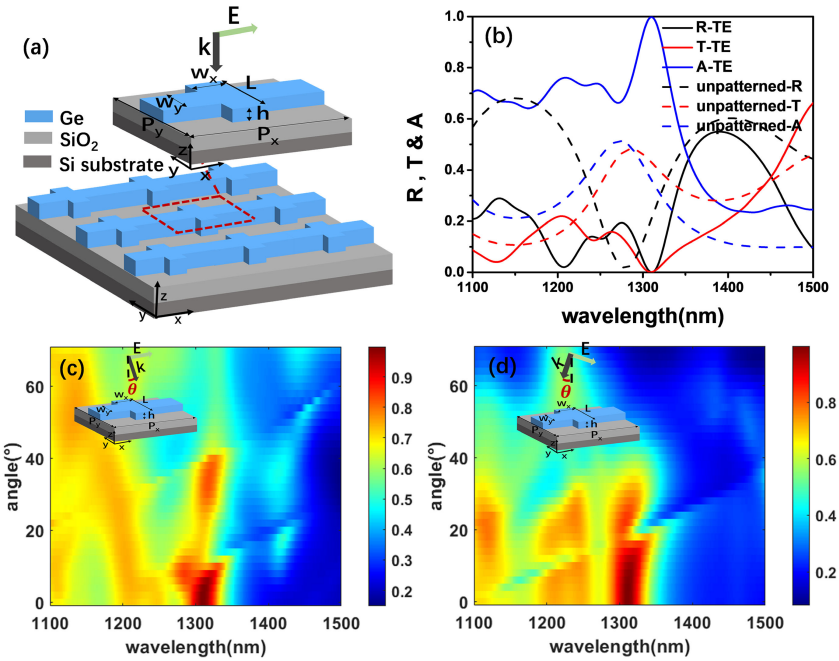

Fig. 3. Substrated Ge waveguide-array-like absorber. (a) Structure configuration. The absorber is put on a standard Si substrate with a 1.04 μm silica spacer. (b) Transmission, reflection and absorption for normal TE incidence. $P_x = P_y = 800$ nm, $w_x = 200$ nm, $L = 590$ nm, $w_y = 310$ nm and $h = 450$ nm. (c) and (d) Influence of incident angle θ on the absorption. In (c), the incident electric field is polarized along the x direction and the inset illustrates the variation of θ. And in (d), the incident magnetic field is polarized along the y direction and the inset illustrates the variation of θ.

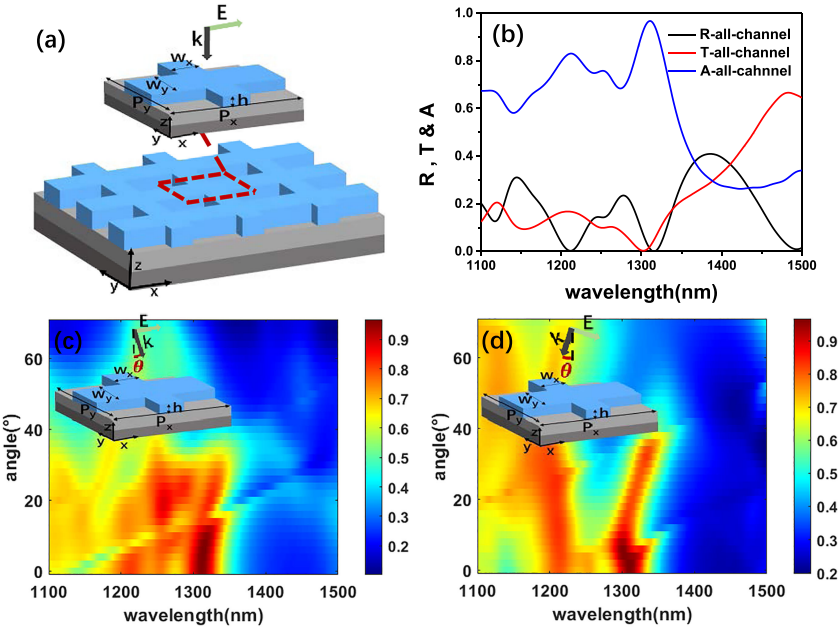

Fig. 4. Substrated Ge all-channel waveguide-array-like absorber. (a) Structure configuration. (b) Transmission, reflection and absorption for normal TE incidence. $P_x = P_y = 830$ nm, $w_x = 160$ nm, $w_y = 310$ nm, $h = 450$ nm. (c) and (d) Influence of incident angle θ on the absorption. In (c), the incident electric field is polarized along the x direction and the inset illustrates the variation of θ. And in (d), the incident magnetic field is polarized along the y direction and the inset illustrates the variation of θ.

incidence of small θ, but it decreases rapidly when θ tends to the first-order diffraction inside the SiO_2 spacer induced by the longitudinal period of P_x.

As an extreme case of the above absorber illustrated in Fig. 3(a), the assistant side arms are lengthened to touch each other to form an all-channel waveguide-array-like absorber ($L = P_y$). Fig. 4(a) shows the schematic diagram of such an extended absorber. Such a bidirectional channel conducting produced carriers may be required in the integration of the suggested absorber with an electrical structure. When the geometrical parameters are set as $P_x = P_y = 830$ nm, $w_x = 160$ nm, $w_y = 310$ nm and $h = 450$ nm, Fig. 4(b) shows the scattering behavior

for normal TE incidence. Perfect absorption is not reached and the strongest absorption is about 96.7% near 1310 nm. However, wideband strong absorption is kept and the absorption between 1100 nm and 1340 nm is over 60%. The scattering behavior for normal TM incidence is also shown as Fig. S1 in the supplementary material, where one can see that perfect absorption can't be achieved in this situation while wideband absorption can still be obtained in a weaker way. Fig. 4(c) and (d) show the variation of the absorption for oblique incidence like the case for the waveguide-array-like absorber investigated above. The absorption of the current absorber displays relatively weak dependence on the incident angle. We have fabricated such an all-channel waveguide-array-like absorber confirming the numerical design (see supplementary material S4).

III. Conclusion

The proposed absorbers have a potential to construct a thin surface-illuminated Ge vertical-PIN photodetector. Such a detector model is illustrated in Fig. S2 in the supplementary material. According to the discussion in supplementary material S3, because the active Ge layer is thin, the detector can achieve a stronger and faster response.

In summary, we have demonstrated a special kind of thin all-dielectric Ge absorbers. The introduction of thin arms enables the perfect absorption for a dielectric waveguide-like array base on mode overlapping. If perfect absorption is not necessary, wideband absorption can also be achieved. The suggested absorbers can make photon detecting possess a higher efficiency and a faster response. Our method is not only enlightened for Ge photodetectors, but also for detection based on other active materials.

References

[1] N. I. Landy, S. Sajuyigbe, J. J. Mock, D. R. Smith, and W. J. Padilla, "Perfect metamaterial absorber," *Phys. Rev. Lett.*, vol. 100, no. 20, 2008, Art. no. 207402.

[2] H. Tao, N. I. Landy, C. M. Bingham, X. Zhang, R. D. Averitt, and W. J. Padilla, "A metamaterial absorber for the terahertz regime: Design, fabrication and characterization," *Opt. Exp.*, vol. 16, no. 10, pp. 7181–7188, 2008.

[3] X. Liu and W. J. Padilla, "Reconfigurable room temperature metamaterial infrared emitter," *Optica*, vol. 4, no. 4, pp. 430–433, 2017.

[4] L. Lei, S. Li, H. Huang, K. Tao, and P. Xu, "Ultra-broadband absorber from visible to near-infrared using plasmonic metamaterial," *Opt. Exp.*, vol. 26, no. 5, pp. 5686–5693, 2018.

[5] Y. Cui et al., "Ultrabroadband light absorption by a sawtooth anisotropic metamaterial slab," *Nano Lett.*, vol. 12, no. 3, pp. 1443–1447, 2012.

[6] Y.-F. C. Chau, C.-T. C. Chao, C. M. Lim, H. J. Huang, and H.-P. Chiang, "Depolying tunable metal-shell/dielectric core nanorod arrays as the virtually perfect absorber in the near-infrared regime," *ACS Omega*, vol. 3, no. 7, pp. 7508–7516, 2018.

[7] E. M. Smith et al., "Epsilon-near-zero thin-film metamaterials for wideband near-perfect light absorption," *Opt. Mater. Exp.*, vol. 10, no. 10, pp. 2439–2446, 2020.

[8] L. Huang et al., "Experimental demonstration of terahertz metamaterial absorbers with a broad and flat high absorption band," *Opt. Lett.*, vol. 37, no. 2, pp. 154–156, 2012.

[9] J. Hendrickson, J. Guo, B. Zhang, W. Buchwald, and R. Soref, "Wideband perfect light absorber at midwave infrared using multiplexed metal structures," *Opt. Lett.*, vol. 37, no. 3, pp. 371–373, 2012.

[10] P. Bouchon, C. Koechlin, F. Pardo, R. Haïdar, and J.-L. Pelouard, "Wideband omnidirectional infrared absorber with a patchwork of plasmonic nanoantennas," *Opt. Lett.*, vol. 37, no. 6, pp. 1038–1040, 2012.

[11] N. Raeis-Hosseini and J. Rho, "Metasurfaces based on phase-change material as a reconfigurable platform for multifunctional devices," *Materials*, vol. 10, no. 9, 2017, Art. no. 1046.

[12] A. K. Chowdhary, T. Bhowmik, and D. Sikdar, "Polarization- and angle-insensitive ultrabroadband perfect metamaterial absorber for thermophotovoltaics," *J. Opt. Soc. Amer. B*, vol. 38, no. 2, pp. 327–335, 2021.

[13] D. Schurig et al., "Metamaterial electromagnetic cloak at microwave frequencies," *Science*, vol. 314, no. 5801, pp. 977–980, 2006.

[14] W. Cai, U. K. Chettiar, A. V. Kildishev, and V. M. Shalaev, "Optical cloaking with metamaterials," *Nature Photon.*, vol. 1, no. 4, pp. 224–227, 2007.

[15] P. Wu, Z. Chen, H. Jile, C. Zhang, D. Xu, and L. Lv, "An infrared perfect absorber based on metal-dielectric-metal multi-layer films with nanocircle holes arrays," *Results Phys.*, vol. 16, 2020, Art. no. 102952.

[16] C. Li et al., "Tunable near-infrared perfect absorber based on the hybridization of phase-change material and nanocross-shaped resonators," *Appl. Phys. Lett.*, vol. 113, no. 23, 2018, Art. no. 231103.

[17] C. Liang et al., "Dual-Band infrared perfect absorber based on a Ag-Dielectric-Ag multilayer films with nanoring grooves arrays," *Plasmonics*, vol. 15, no. 1, pp. 93–100, 2020.

[18] M. A. Shameli and L. Yousefi, "Absorption enhancement in thin-film solar cells using an integrated metasurface lens," *J. Opt. Soc. Amer. B*, vol. 35, no. 2, pp. 223–230, 2018.

[19] J. Krügener et al., "Photonic crystals for highly efficient silicon single junction solar cells," *Sol. Energy Mater. Sol. Cells*, vol. 233, 2021, Art. no. 111337.

[20] A. K. Azad et al., "Metasurface broadband solar absorber," *Sci. Rep.*, vol. 6, no. 1, 2016, Art. no. 20347.

[21] N. Liu, M. Mesch, T. Weiss, M. Hentschel, and H. Giessen, "Infrared perfect absorber and its application as plasmonic sensor," *Nano Lett.*, vol. 10, no. 7, pp. 2342–2348, 2010.

[22] M. Askari, "A near infrared plasmonic perfect absorber as a sensor for hemoglobin concentration detection," *Opt. Quantum Electron.*, vol. 53, no. 2, 2021, Art. no. 67.

[23] Z. Yi et al., "Dual-band plasmonic perfect absorber based on graphene metamaterials for refractive index sensing application," *Micromachines*, vol. 10, no. 7, 2019, Art. no. 443.

[24] S. Fan and J. D. Joannopoulos, "Analysis of guided resonances in photonic crystal slabs," *Phys. Rev. B*, vol. 65, no. 23, 2002, Art. no. 235112.

[25] A. A. Erchak et al., "Enhanced coupling to vertical radiation using a two-dimensional photonic crystal in a semiconductor light-emitting diode," *Appl. Phys. Lett.*, vol. 78, no. 5, pp. 563–565, 2001.

[26] X. Cao, Y. Zhang, Z. Han, W. Li, Y. Jin, and A. Wu, "Enhancing the absorption of a thin germanium slab with periodical patterning," *J. Mater. Sci.: Mater. Electron.,* vol. 31, no. 8, pp. 5872–5878, 2020.

[27] Z.-X. Zhou et al., "Germanium metasurfaces with lattice kerker effect in near-infrared photodetectors," *ACS Nano*, vol. 16, no. 4, pp. 5994–6001, 2022.

[28] Y. Wang et al., "All-dielectric terahertz plasmonic metamaterial absorbers and high-sensitivity sensing," *ACS Omega*, vol. 4, no. 20, pp. 18645–18652, 2019.

[29] O. Mitrofanov et al., "Perfectly absorbing dielectric metasurfaces for photodetection," *APL Photon.*, vol. 5, no. 10, 2020, Art. no. 101304.

[30] H. Ito, S. Kodama, Y. Muramoto, T. Furuta, T. Nagatsuma, and T. Ishibashi, "High-speed and high-output InP-InGaAs unitraveling-carrier photodiodes," *IEEE J. Sel. Top. Quantum Electron.,* vol. 10, no. 4, pp. 709–727, Jul./Aug. 2004.

[31] N. Shimizu, N. Watanabe, T. Furuta, and T. Ishibashi, "InP-InGaAs unitraveling-carrier photodiode with improved 3-dB bandwidth of over 150 GHz," *IEEE Photon. Technol. Lett.*, vol. 10, no. 3, pp. 412–414, Mar. 1998.

[32] S. B. Samavedam, M. T. Currie, T. A. Langdo, and E. A. Fitzgerald, "High-quality germanium photodiodes integrated on silicon substrates using optimized relaxed graded buffers," *Appl. Phys. Lett.*, vol. 73, no. 15, pp. 2125–2127, 1998.

[33] E. D. Palik, *Handbook of Optical Constants of Solids*. Boston, MA, USA: Academic Press, 1998.

[34] B. Yang et al., "Ultrahighly saturated structural colors enhanced by multipolar-modulated metasurfaces," *Nano Lett.*, vol. 19, no. 7, pp. 4221–4228, 2019.

[35] Q. Li, J. van de Groep, Y. Wang, P. G. Kik, and M. L. Brongersma, "Transparent multispectral photodetectors mimicking the human visual system," *Nature Commun.*, vol. 10, no. 1, 2019, Art. no. 4982.

[36] C.-Y. Yang et al., "Nonradiating silicon nanoantenna metasurfaces as narrowband absorbers," *ACS Photon.*, vol. 5, no. 7, pp. 2596–2601, 2018.